Synthesis and Property Characterization of Ternary Laminar Zr2SB Ceramic

Qiqiang Zhang
Southwest Jiaotong University
Shuai Fu
China Building Materials Academy
Detian Wan
China Building Materials Academy
Yiwang Bao
China Building Materials Academy
Qingguo Feng
Southwest Jiaotong University
Salvatore Grasso
Southwest Jiaotong University
Chunfeng Hu (chfhu@live.cn)
Southwest Jiaotong University https://orcid.org/0000-0003-0882-9916

Research Article

Keywords: Zr2SB, Spark plasma sintering, Reaction path, Microstructure, Properties

Posted Date: October 26th, 2021

DOI: https://doi.org/10.21203/rs.3.rs-982056/v1

Version of Record: A version of this preprint was published at Journal of Advanced Ceramics on April 2nd, 2022. See the published version at https://doi.org/10.1007/s40145-022-0577-3.

Synthesis and Property Characterization of Ternary Laminar Zr_2SB Ceramic

Qiqiang Zhang[1], Shuai Fu[2], Detian Wan[2], Yiwang Bao[2], Qingguo Feng[1], Salvatore Grasso[1], Chunfeng Hu[1,*]

[1]*Key Laboratory of Advanced Technologies of Materials, Ministry of Education, School of Materials Science and Engineering, Southwest Jiaotong University, Chengdu 610031, China*

[2]*State Key Laboratory of Green Building Materials, China Building Materials Academy, Beijing 100000, China*

Abstract

In this paper, Zr_2SB ceramics with high relative density (99.03%) and high purity of 82.95 wt% (containing 8.96 wt% ZrB_2 and 8.09 wt% zirconium) were successfully synthesized from ZrH_2, sublimated sulfur and boron powder by spark plasma sintering at 1300 ℃. The reaction mechanism, microstructures, physical properties and mechanical properties of Zr_2SB ceramic were systematically studied. The results show that Zr_2SB was obtained by the reaction of zirconium sulfide, zirconium and boron, and ZrB_2 coexisted in the sample as a symbiotic impurity phase. The average grain size of Zr_2SB was 12.46 μm in length and 5.12 μm in width, and the mean grain sizes of ZrB_2 and zirconium impurities were about 300 nm. In terms of physical properties, the measured thermal expansion coefficient was 7.64×10^{-6} K^{-1} from room temperature to 1200 ℃, and the thermal capacity and thermal conductivity at room temperature were 0.39 $J \cdot g^{-1} \cdot K^{-1}$ and 12.01 $W \cdot m^{-1} \cdot K^{-1}$, respectively. The room temperature electrical conductivity of Zr_2SB ceramic was measured to be 1.74×10^6 $\Omega^{-1} \cdot m^{-1}$. In terms of mechanical properties, Vickers hardness was 9.86 ± 0.63 GPa under 200 N load, and the measured flexural strength, fracture toughness and compressive strength were 269 ± 12.7 MPa, 3.94 ± 0.63 $MPa \cdot m^{1/2}$, and 2166.74 ± 291.34 MPa, respectively.

Keywords: Zr_2SB; Spark plasma sintering; Reaction path; Microstructure; Properties

*Corresponding author: Prof. Chunfeng Hu
School of Materials Science and Engineering
Southwest Jiaotong University, Chengdu 610031, China
E-mail address: chfhu@live.cn

1. Introduction

$M_{n+1}AX_n$ phase (n = 1–3) is a kind of ternary layered compounds, in which the M element is the early transition metal, the A element is the main group element (12–16) and the X element is B, C or N. MAX phase was first proposed by Nowotny *et al*. [1] in the 1960s. Barsoum *et al*. [2] synthesized the bulk Ti_3SiC_2 ceramics through hot pressing and reported on a range of unique properties including high thermal conductivity, high flexural strength, high fracture toughness, excellent machinability and etcetera. These excellent properties [2 – 4] are attractive to researchers to conduct extensive researches. So far, more than 650 MAX phases have been calculated as thermodynamically stable, but only about 160 MAX phases have been successfully synthesized [5,6].

Most recently, boron has been found to be a X element of MAX phase. It should be noted that MAX phase boride is not MAB phase. According to the First-principles calculation, the MAX phase boride has a typical MAX phase structure that the M_6B octahedral layers are interleaved with the A element layers [3,7], while the M_6B unit in the MAB phase has a completely different structure of trigonal prism. Especially, there are B-B bonds in MAB phase, but not in MAX phase. The known MAB phases include MAlB (M = Mo, W) phase, M_2AlB_2 (M = Mn, Cr, Fe) phase, $M_5Si_3B_x$ (M = Cr, Hf) phase [8 – 10] and etcetera. Like MAX phase, MAB phase also has a series of interesting properties.

Most initial studies of MAX phase borides started from the corresponding carbide MAX phase. Chakrabotry *et al.* [7] simulated the properties of V_2AlC/V_2AlB and judged that the introduction of boron can effectively enhance the ductility. At present, there are mature studies on the synthesis, characterization and calculation of M_2SC (M = Ti, Zr, Nb, Hf) [11 – 21]. Based on the research on M_2SC, Ali *et al*. [22] simulated the lattice structure and physical properties of M_2SC and M_2SB (M = Zr, Hf, Nb), identified that M_2SB phases have dynamical stability and revealed the application prospect of Zr_2SB in reducing solar absorption coating. Rackl *et al*. [23,24] were the first to synthesize the MAX phase $Nb_2S(B,C)$ and Nb_2SB powders by solid

phase reaction methods and applied similar processes to synthesize Hf_2SB and Zr_2SB phases. They reported that the substitution of boron for carbon could increase the cell size and reduce the deformation of $Nb_6(B,C)$ octahedron. Qin *et al.* [25] successfully synthesized compact and pure Nb_2SB for the first time and tested a series of mechanical and physical properties.

To date, the literature on MAX phase boride, especially M_2SB phase has focused mainly on crystal structure, electron distribution and physical properties and less is known about the mechanical strength. To tackle this void, we rapidly prepared dense Zr_2SB ceramics by spark plasma sintering (SPS) and explored a series of physical and mechanical properties.

2. Experimental procedure

This experiment used commercial zirconium hydride (99.9% purity, 300 mesh) (NAIOU nano-technology Co., Ltd., China), sublimated sulfur (99.9% purity, 200 mesh) (WANYU pharmaceutical Co., Ltd., China), boron (99% purity, 5um) (ENO high tech material development Co., Ltd., China) as the initial powders. The powder mixtures with different molar ratio were weighed on an electronic scale (accurate to 10^{-4} g) and ball-milled on a rotating machine at 50 rpm for 12 hours. These powder mixtures were loaded into a Ø20 mm cylindrical graphite mold and sintered in a spark plasma sintering furnace (SPS-20T-10, Chenhua Technology Co., Ltd., China) at a preset heating rate and pressure. In this preset sintering step, the heating rate below 700 ℃ was set as 50 ℃/min and the pressure was set as 20 MPa; the heating rate above 700 ℃ was set as 10 ℃/min and the pressure was set as 30 MPa. After sintering, we cooled the sample to 900 ℃ at a rate of 50 ℃/min and then cooled with the furnace.

The phase composition was determined by X-ray diffraction (D8 advance, Bruker, Germany) with a Cu-Kα radiation (λ = 1.54178Å) source and the scanning speed was set to 0.02°/step. The fracture surface of bulk Zr_2SB ceramic was observed by a field emission scanning electron microscope (Apreo 2C, Thermo Fisher Scientific, The

Czech Republic). Energy dispersive spectroscopy (EDS) was also used to determine the composition of fracture surfaces.

The coefficient of thermal expansion (TEC) was tested in argon environment using a thermal expansion analyzer (L75HD1600C, Netzsch, Germany) with a temperature range of 200-1200 ℃ and a heating rate of 5 ℃/min. The sample size was 4 × 4 × 15 mm^3. The thermal properties were tested in vacuum with a laser thermal conductivity meter (LFA467, Netzsch, Germany) in the temperature range of 25 – 1200 ℃. The sample size was Ø12.5 × 3 mm^3. The conductivity of Zr_2SB was measured at room temperature by a resistivity tester (FT-300A1, Ningbo Rooko Instrument Co., Ltd., China) with a sample size of 1×1×10 mm^3.

Vickers hardness of Zr_2SB ceramic under 1 – 200 N loads was tested by a micro-hardness tester (HVS-1000ZA, Wanheng Corp., China and HVS-50, Lianer Corp., China) and measured five times for each load point. The flexural strength, fracture toughness and compressive strength of Zr_2SB ceramic were tested by a universal testing machine and the sample sizes were $1.5 \times 2 \times 18\ mm^3 (GB/T\ 6569-2006), 2 \times 4 \times 18\ mm^3 (GB/T\ 23806-2009)$, and $2 \times 2 \times 4\ mm^3 (GB/T\ 8489-2006)$ respectively. The flexural strength was obtained by the three-point bending method, and the fracture toughness was obtained by single-edge notched beam method (SENB) with the notch of 2 mm in length and 0.3 mm in width. The span of flexural strength experiment and fracture toughness experiment was set to 16 mm. The cross-head speed in the three mechanical properties was set to 0.5 mm/min.

3. Results and discussion

3. 1 Reaction mechanisms

To study the reaction mechanism, this work used commercial purchased zirconium hydride, sublimated sulfur and boron powders as initial materials to investigate the reaction path. Fig. 1. (a) – (h) are the X-ray diffraction (XRD) patterns of the samples

obtained by spark plasma sintering (SPS) at sintering temperatures of 650 ℃, 800 ℃, 900 ℃, 1000 ℃, 1100 ℃, 1200 ℃, 1300 ℃ and 1400 ℃, respectively. For ease of analysis, the phase compositions of the samples at each temperature are summarized in Table 1.

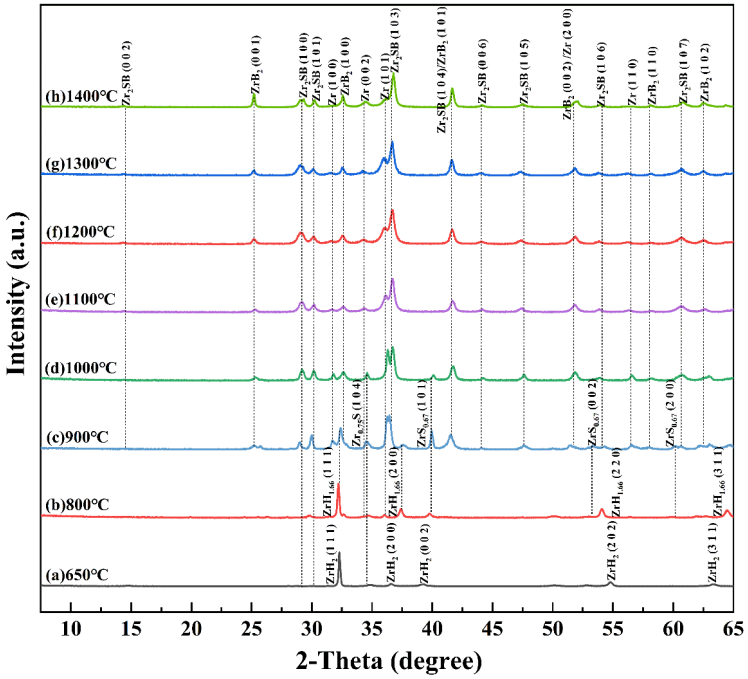

Fig. 1 X-ray diffraction (XRD) patterns of Zr_2SB ceramic at different sintering temperatures of (a) 650 ℃, (b) 800 ℃, (c) 900 ℃, (d) 1000 ℃, (e) 1100 ℃, (f) 1200 ℃, (g) 1300 ℃, and (h) 1400 ℃.

Table 1 Phase compositions of Zr_2SB ceramic sintered by SPS at different sintering temperatures

Temperature	Phase composition
650 ℃	ZrH_2, $Zr_{0.75}S$
800 ℃	$ZrH_{1.66}$, Zr, $Zr_{0.75}S$, $ZrS_{0.67}$
900 ℃	$ZrH_{1.66}$, Zr, $Zr_{0.75}S$, $ZrS_{0.67}$, ZrB_2, Zr_2SB
1000 ℃	Zr, $Zr_{0.75}S$, $ZrS_{0.67}$, ZrB_2, Zr_2SB
1100 ℃, 1200 ℃, 1300 ℃, 1400 ℃	Zr, ZrB_2, Zr_2SB

Results showed that ZrH_2 decomposed into $ZrH_{1.66}$ and released hydrogen below

800 ℃, while $ZrH_{1.66}$ completely decomposed into zirconium at about 1000 ℃. At the same time, the sulfur gasified at 444.6 ℃ and reacted with hydrogen reversibly. The degree of reversible reaction depended on the reaction conditions. The reaction equations were probably as follows:

$$6ZrH_2(s) \rightarrow 6ZrH_{1.66}(s) + H_2(g) \quad (1)$$

$$6ZrH_{1.66}(s) \rightarrow 6Zr(s) + 5H_2(g) \quad (2)$$

$$S(g) + H_2(g) \rightleftharpoons H_2S(g) \quad (3)$$

Zirconium obtained from the decomposition of ZrH_2 reacted with sulfur at 650 ℃ to form $Zr_{0.75}S$. The increase of temperature accelerated the decomposition of ZrH_2 and formed a large amount of $Zr_{0.75}S$ and $ZrS_{0.67}$ sulfides (the low-intensity unmarked peaks at 800 ℃ and 900 ℃ were diffraction peaks of a mixture of zirconium sulfides). The reaction was most vigorous at 900 ℃, and the reaction equations were:

$$3Zr(s) + 4S(g) \rightarrow 4Zr_{0.75}S(s) \quad (4)$$

$$3Zr(s) + 2S(g) \rightarrow 3ZrS_{0.67}(s) \quad (5)$$

ZrB_2 was generated above 900 ℃. As the sintering temperature increased, the amount of ZrB_2 generated increased gradually and reached a maximum at 1200 ℃, that is, boron was completely consumed at 1200 ℃. The reaction equation was:

$$Zr(s) + 2B(s) \rightarrow ZrB_2(s) \quad (6)$$

At 900 ℃, the sulfur in the raw material had been sublimated and there was no large amount of ZrB_2 produced. Therefore, we considered that Zr_2SB was formed by the reaction of zirconium sulfide, zirconium and boron. The X-ray diffraction patterns showed that the content of Zr_2SB reached the highest value at a sintering temperature of 1200 ℃, at which the reaction had proceeded completely. And the density of samples increased while the sintering temperature increased from 1200 ℃ to 1300 ℃. The reaction equations were:

$$3ZrS_{0.67}(s) + Zr(s) + 2B(s) \rightarrow 2Zr_2SB(s) \quad (7)$$

$$4Zr_{0.75}S(s) + 5Zr(s) + 4B(s) \rightarrow 4Zr_2SB(s) \quad (8)$$

At 1400 ℃, we observed a metallic shiny solid adhering to the indenter of the graphite mold, which resulted in the loss of part of the material. According to the

X-ray diffraction patterns, we believed that the main component of this material is zirconium. That means, at 1400 ℃, Zr_2SB decomposed, the sulfur layer departed from the MAX phase, and generated zirconium with ZrB_2. The reaction equation is:

$$2Zr_2SB(s) \rightarrow ZrB_2(s) + 3Zr(s) + 2S(g) \quad (9)$$

The sublimated sulfur would suffer gasification loss at normal temperature, and the sulfur would also react with the hydrogen released by the reaction during heating. This loss of sulfur would result in a portion of zirconium and ZrB_2 remaining after sintering the powder mixed at standard stoichiometry. Therefore, we further adjusted the sulfur proportion to confirm the appropriate sulfur ratio and the corresponding process under the experimental conditions.

3. 2 Formula modification

According to the reaction path studied above, a holding temperature lower than 800 ℃ can not only increase the formation of zirconium sulfide, but also control the formation of impurities (zirconium boride), thereby improving the purity of the obtained samples. Therefore, we used a sintering temperature of 1300 ℃ and kept it at 700 ℃ for 10 minutes to adjust the proportion of sulfur to explore the most appropriate relative proportion. A series of relative proportions were selected according to the impurity content, and the results are shown in Fig. 2. (a) – (f).

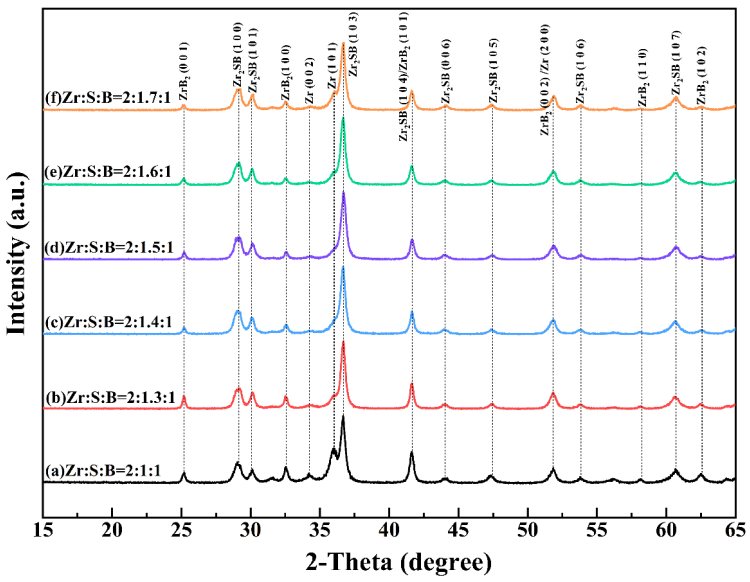

Fig. 2 XRD patterns with different sulfur proportion of ZrH_2 : S : B = (a) 2 : 1 : 1, (b) 2 : 1.3 : 1, (c) 2 : 1.4 : 1, (d) 2 : 1.5 : 1, (e) 2 : 1.6 : 1, and (f) 2 : 1.7 : 1.

It is obvious that with the increase of sulfur addition, zirconium and ZrB_2 in the sample have a significant downward trend and reach the minimum value at ZrH_2 : S : B = 2 : 1.6 : 1. With the increase of sulfur proportion, the decreasing trend of zirconium and ZrB_2 gradually slowed down. This phenomenon was due to the addition of excess sulfur. The increase in the vapor pressure of volatile sulfur in the mold made the reversible reaction of hydrogen and sulfur more complete, and more sulfur escaped in the form of hydrogen sulfide.

When the formula was 2 : 1.7 : 1, we observed that when the temperature raised about 300 ℃, a large amount of gas escaped from the mold, and the furnace vacuum dropped rapidly. This was because the volatile sulfur and hydrogen released by the decomposition of zirconium hydride made the pressure in the mold too high, and the gas escaped from the gap of the mold. As a result, the sulfurs involved in the reaction decreased and the content of zirconium and ZrB_2 in the sample increased abnormally.

Based on the results of these experiments, we can confirm that zirconium sulfides played an important role in the formation of Zr_2SB and the loss of sulfur is the main reason for the existence of impurity phases ZrB_2 and zirconium. As a rapid sintering method, SPS [26 – 31] can control the escape of sulfur and purify samples as much as possible, but the sintering of Zr_2SB is still difficult. In our experiment, the best relative ratio of sulfur under these experimental conditions were 1.6. However, since there are still a large amount of zirconium and ZrB_2 in the sample, we'd like to adjust the ratio of zirconium and boron to obtain higher purity samples.

To further purify the sample, we first adjusted the formula of zirconium. Under the condition of a sintering temperature of 1300 ℃ and relative sulfur ratio of 1.6, the results obtained by adjusting the addition amount of ZrH_2 are shown in Fig. 3. (a) – (f).

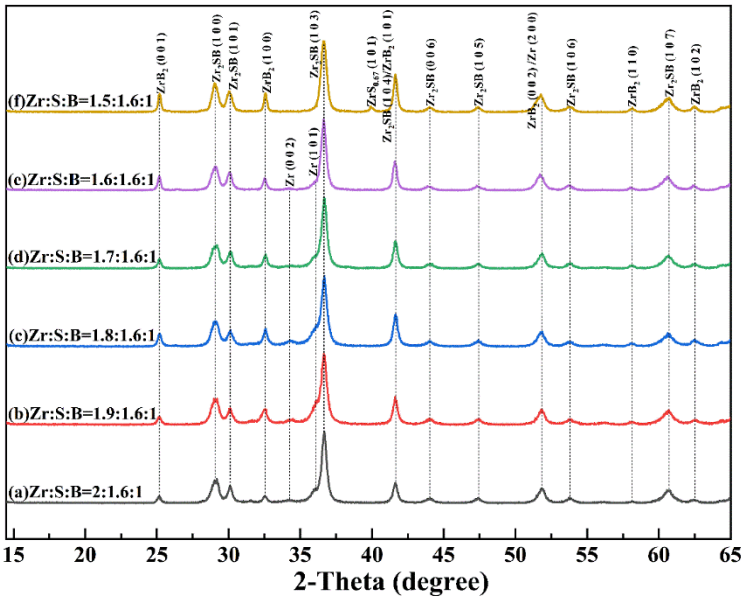

Fig. 3 XRD patterns with different ZrH_2 proportion, ZrH_2 : S : B = (a) 2 : 1.6 : 1, (b) 1.9 : 1.6 : 1, (c) 1.8 : 1.6 : 1, (d) 1.7 : 1.6 : 1, (e) 1.6 : 1.6 : 1, and (f) 1.5 : 1.6 : 1.

Figure 3 depicts the gradual decrease of zirconium in the sample as the content of ZrH_2 decreases. Specifically, when the relative ratio of ZrH_2 is 1.6, the peak of zirconium almost disappears. When the relative ratio of ZrH_2 is 1.5, the peak of zirconium disappears completely and the peak of $ZrS_{0.67}$ appears. The simultaneous existence of $ZrS_{0.67}$ and ZrB_2 proves that ZrB_2 does not react with zirconium sulfide to form Zr_2SB, which is an impurity phase generated during the reaction. This also indicates that zirconium sulfide may be an ideal precursor of Zr_2SB, but due to the limited experimental conditions, this method has not been applied in this paper. Meanwhile, the content of ZrB_2 increases obviously with the decrease of ZrH_2. This is because the excess of boron leads to a strong tendency to form ZrB_2. Therefore, we further adjusted the boron proportion based on the molar ratio of ZrH_2 : S : B = 1.6 : 1.6 : 1.

It can be seen from Fig. 4. that the ratio of zirconium hydride to boron has a great impact on the purity of the sample, and the best ratio of ZrH_2 : B is 2 : 1. Therefore, we coordinated the adjustment of these two raw materials, and finally obtained the purest sample with ZrH_2 : S : B of 1.4 : 1.6 : 0.7. The XRD data of the obtained

samples are shown in Figure 5, and the spectrum is similar to that obtained by Tobias Rackl *et al*. [24]. Based on their work, we further incorporated zirconium into the Rietveld refinement, which is shown in Figure 5. According to the Rietveld refinement results, the sample is composed of 82.95 wt% Zr_2SB, 8.96 wt% ZrB_2 and 8.09 wt% zirconium.

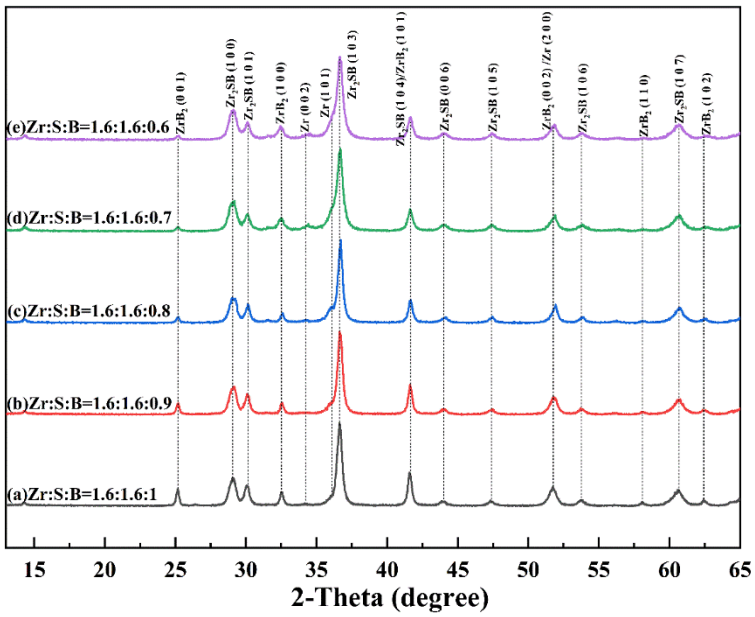

Fig. 4 XRD patterns with different boron proportion, ZrH_2 : S : B = (a) 1.6 : 1.6 : 1, (b) 1.6 : 1.6 : 0.9, (c) 1.6 : 1.6 : 0.8, (d) 1.6 : 1.6 : 0.7, and (e) 1.6 : 1.6 : 0.6.

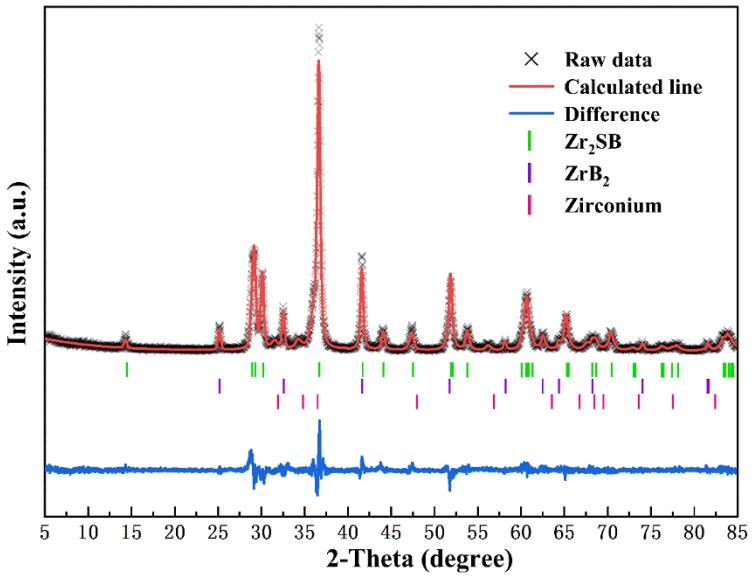

Fig. 5 Comparison between the observed (black cross) and calculated (red curve) XRD patterns. The blue curve represents the difference between the observed and calculated XRD patterns. Green, purple and pink marks are the peak positions of Zr_2SB, ZrB_2 and zirconium respectively.

3. 3 Microstructure characterization

The density of Zr_2SB sample measured by the Archimedes' method is 6.13 g/cm^3 and the theoretical density including impurity content is 6.19 g/cm^3, corresponding to the densification of 99.03%. Figure 6 is the scanning electron microscope (SEM) image and the energy dispersive spectrometer (EDS) result of the flexural fracture surface of Zr_2SB. The EDS results confirm that the Zr : S ratio of the larger grain in this sample is about 1.85, which is within the allowable error range. Thus, we believe that the larger grain in the sample is Zr_2SB. We selected 30 crystal grains with clear boundaries on the concave fracture surface for grain size calculation. The grain size of Zr_2SB is larger than that of Nb_2SB (6 μm in length and 3.6 μm in width) sintered with SPS, with an average length of 12.46 μm and an average width of 5.12 μm. The impurity phases ZrB_2 and zirconium are distributed at the grain boundaries of lath shaped Zr_2SB, and the average grain size of both impurities is 300 nm.

Intergranular/transgranular fracture occurred in Zr_2SB grains. Many transgranular fractured Zr_2SB grains with obvious layered characteristics can be observed on both concave and convex fractures. Meanwhile, pits left after the grains fall off due to intergranular fracture can be observed on the concave fracture, and the corresponding detached complete grains can be observed on the convex surface. Intergranular fracture exists in the ZrB_2 and zirconium impurity grains. And due to the low strength of the impurity grain boundary, the cracks expand rapidly at these positions, resulting in that the bending strength and fracture toughness test results of this sample will be slightly lower than the actual values.

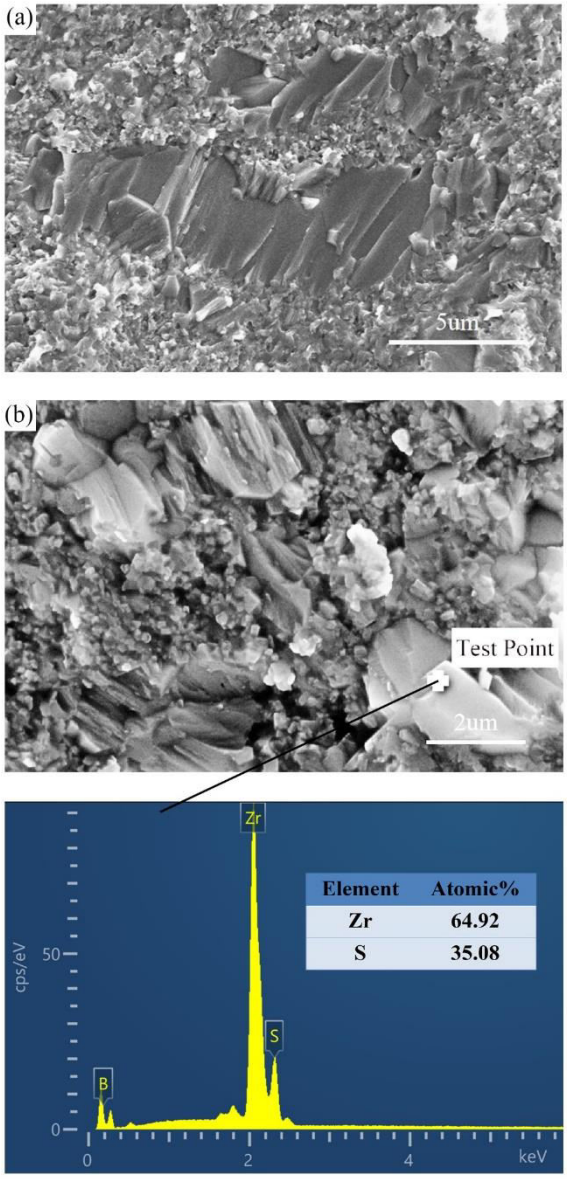

Fig. 6 Scanning electron microscope (SEM) images of Zr_2SB flexural fracture surface: (a) concave fracture surface and (b) convex fracture surface; (c) energy dispersive spectrometer (EDS) result of Zr_2SB grains.

3. 4 Physical properties evaluation

The red curve in Fig. 7. is the thermal expansion curve of Zr_2SB measured at 25 ℃ to 1200 ℃, and the black line is the result of linear fitting. The equation is $\alpha_{\mathrm{TEC},1200\,℃} = -0.01147 + 0.00078337\mathrm{T}$ with the R-square of 0.99417. The average thermal expansion coefficient (TEC) of Zr_2SB is calculated as $7.64 \times$

$10^{-6}\ K^{-1}$, which is between Zr_2SC ($8.8 \times 10^{-6}\ K^{-1}$) [21] and Nb_2SB ($7.1 \times 10^{-6}\ K^{-1}$) [25].

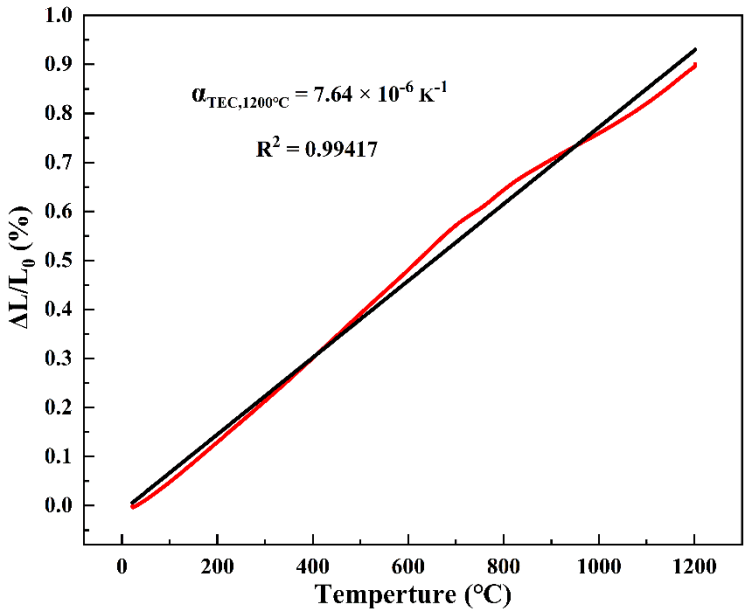

Fig. 7 Thermal expansion (red curve) and linear fitting result (black straight line) of Zr_2SB ceramic at 25 ℃ to 1200 ℃.

Fig. 8. is the temperature dependence of thermal diffusivity. The thermal diffusion coefficient increases from 4.97 mm^2/s at room temperature to 7.29 mm^2/s at 1200 ℃. Compared with Nb_2SB, the thermal diffusion coefficient of Zr_2SB is smaller in the same temperature range, and maintains at a very low value. Figure 9 shows the temperature dependence of thermal conductivity and heat capacity of Zr_2SB ceramic sintered by SPS. The thermal conductivity of Zr_2SB increases rapidly from 12.0 $W\cdot m^{-1}\cdot K^{-1}$ at room temperature to 30.7 $W\cdot m^{-1}\cdot K^{-1}$ at 800 ℃. As the temperature continues to rise, the change trend slows down obviously and tends to a constant value of 34.2 $W\cdot m^{-1}\cdot K^{-1}$ at 1200 ℃. The thermal conductivity of Zr_2SB at room temperature is lower than those of Nb_2SB (13.79 $W\cdot m^{-1}\cdot K^{-1}$) [25] and Zr_2SC (38 $W\cdot m^{-1}\cdot K^{-1}$ at 100 ℃) [21]. However, as the temperature increases, the thermal conductivity of Zr_2SB (16.7 $W\cdot m^{-1}\cdot K^{-1}$) exceeds that of Nb_2SB at 200 ℃ (15.0 $W\cdot m^{-1}\cdot K^{-1}$). At high temperature, the thermal conductivity of Zr_2SB (34.2 $W\cdot m^{-1}\cdot K^{-1}$

at 1200 ℃) is very close to that of Zr_2SC (34.6 $W \cdot m^{-1} \cdot K^{-1}$ at 1200 ℃). Similarly, the heat capacity of Zr_2SB increases rapidly from 0.39 $J \cdot g^{-1} \cdot K^{-1}$ at room temperature to 0.73 $J \cdot g^{-1} \cdot K^{-1}$ at 600 ℃, and then slowly increases to a constant value of 0.78 $J \cdot g^{-1} \cdot K^{-1}$ at 1200 ℃. At the room temperature, the heat capacity of Zr_2SB is lower than that of Zr_2SC (0.48 $J \cdot g^{-1} \cdot K^{-1}$), while at about 400 ℃, the heat capacity of Zr_2SB (0.58 $J \cdot g^{-1} \cdot K^{-1}$) exceeds that of Zr_2SC (0.53 $J \cdot g^{-1} \cdot K^{-1}$). Also, at high temperatures, the heat capacity of Zr_2SB (0.78 $J \cdot g^{-1} \cdot K^{-1}$ at 1200 ℃) is significantly higher than that of Zr_2SC (0.50 $J \cdot g^{-1} \cdot K^{-1}$ at 1000 ℃). Compared with Zr_2SB and Zr_2SC, the heat capacity of Nb_2SB is relatively low (0.36 $J \cdot g^{-1} \cdot K^{-1}$ at room temperature, 0.49 $J \cdot g^{-1} \cdot K^{-1}$ at 800 ℃).

In addition, the room temperature electrical conductivity of Zr_2SB ceramic was measured to be 1.74×10^6 $\Omega^{-1} \cdot m^{-1}$, which is nearly 50% higher than the room temperature electrical conductivity of Nb_2SB (1.17×10^6 $\Omega^{-1} \cdot m^{-1}$), and slightly lower than the room temperature electrical conductivity of Ti_2SC (1.85×10^6 $\Omega^{-1} \cdot m^{-1}$) [12].

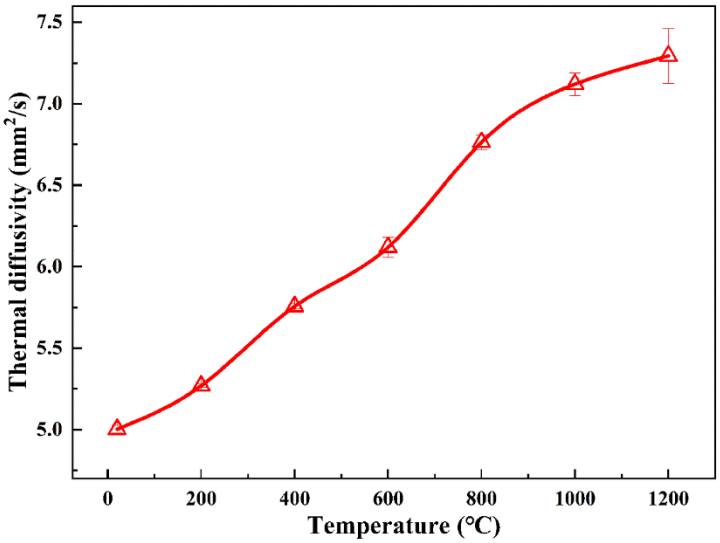

Fig. 8 Thermal diffusivity of Zr_2SB ceramic measured from 20 ℃ to 1200 ℃.

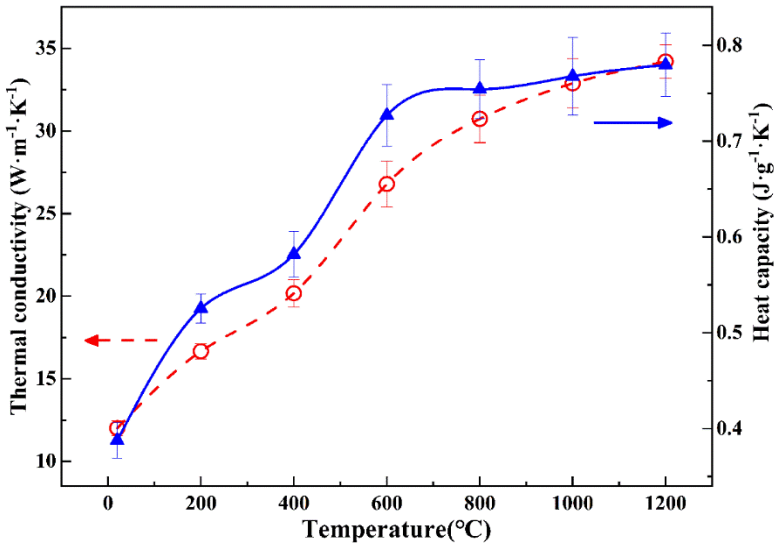

Fig. 9 Thermal conductivity and thermal capacity of Zr_2SB ceramic measured from 20 ℃ to 1200 ℃.

3. 5 Mechanical properties evaluation

Table 2 lists a series of physical and mechanical properties of Zr_2SB sintered by SPS, and compares these properties with Nb_2SB [13] and Zr_2SC [12] sintered by the same method. It should be mentioned that the flexural strength and fracture toughness measured by Zr_2SB are relatively smaller than those of theoretical values because that the impurity phase with low strength exists at the grain boundary. For more details, the measured flexural strength of Zr_2SB is 269 ± 12.7 MPa, which is higher than that of the same type of Nb_2SB (249 ± 17 MPa), close to that of Zr_2SC (275 ± 10 MPa), and much lower than that of Ti_2SC (394 MPa) [14]. The fracture toughness of Zr_2SB is 3.94 ± 0.63 MPa·$m^{1/2}$, slightly lower than those of Nb_2SB (4.76 ± 0.36 MPa·$m^{1/2}$) and Ti_2SC (5.4 MPa·$m^{1/2}$). In addition, the measured compression strength of Zr_2SB samples is 2166.74 ± 291.34 MPa, which is much higher than those of Nb_2SB (1157 ± 73 MPa) and Ti_2SC (736 MPa) sintered by SPS. This is because a large number of small grain impurities at the grain boundary hinder the sliding of Zr_2SB grains and increase the compressive strength of the sample. Nevertheless, its compressive strength is still much higher than that of conventional MAX phases, thus performing good compression performance.

Table 2 Comparison of physical and mechanical properties of Zr_2SB, Nb_2SB and Zr_2SC

Properties	Zr_2SB	Nb_2SB [25]	Zr_2SC [21]
Molecular weight (g/mol)	225.32	228.67	226.5
Density (g/cm^3)	6.17	6.84	-
Flexural strength (MPa)	269 ± 12.7	249 ± 17	275 ± 10
Fracture toughness ($MPa \cdot m^{1/2}$)	3.94 ± 0.63	4.76 ± 0.36	-
Compressive strength (MPa)	2166.74 ± 291.34	1157 ± 73	-
Vickers hardness (GPa) (200 N)	9.86 ± 0.63	12.0	6.4
Electrical conductivity ($\times 10^6\ \Omega^{-1} \cdot m^{-1}$) (25°C)	1.74	1.17	-
Thermal expansion coefficient ($\times 10^{-6}\ K^{-1}$)	7.64	7.1	8.8
Heat capacity, Cp ($J \cdot g^{-1} \cdot K^{-1}$) (25°C)	0.39	0.36	0.4 (100 °C)
Thermal conductivity ($W \cdot m^{-1} \cdot K^{-1}$) (25°C)	12.01	13.79	38 (100 °C)

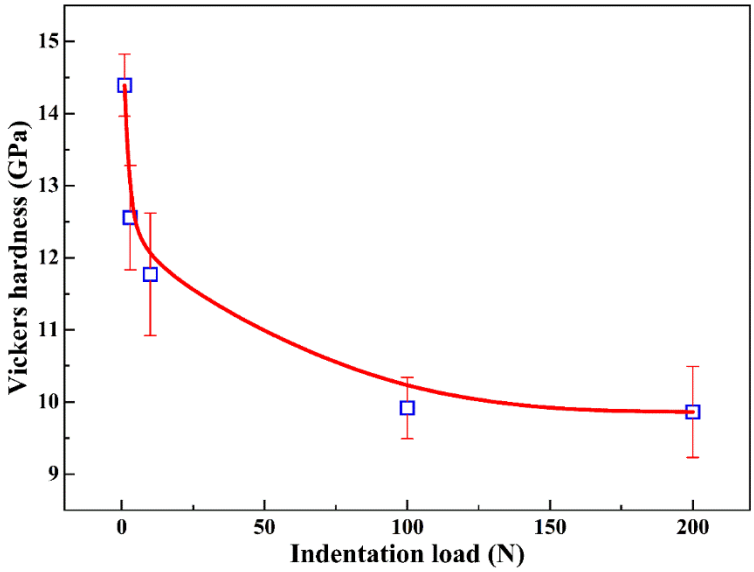

Fig. 10 Vickers hardness as a function of indentation load.

Figure 10 depicts the relationship between the hardness of Zr_2SB and the indentation load. The Vickers hardness is 14.39 ± 0.43 GPa at 1 N load. As the pressure increases, the hardness gradually increases and reaches a constant point of 9.86 ± 0.63 GPa at 200 N load. At a load of 10 N, the hardness of Zr_2SB is 12.55 ± 0.72 GPa, which is higher than that of Nb_2SB (11.89 ± 0.37 GPa), Zr_2SC (6.4 GPa), and Ti_2SC (6.7 GPa). Due to the high hardness and low fracture toughness of Zr_2SB,

cracks appeared at the four corners of the indent. The overall indentation is complete without grain extrusion, and there were no crack extensions at the four corners which would affect the indentation size. Therefore, Zr_2SB, due to its high hardness value corresponding to its good mechanical properties, is currently one of the MAX phases that are most promising to develop into structure-functional ceramics at present.

4. Conclusions

Highly dense boron containing MAX phase Zr_2SB was successfully prepared by SPS, and the corresponding reaction mechanisms, microstructure, physical and mechanical properties of the samples were investigated. The following results were obtained:

(1) The optimum ratio to synthesize Zr_2SB is ZrH_2 : S : B = 1.4 : 1.6 : 0.7 with the process of holding time of 10 min at 700 ℃ and the 10 min at 1300 ℃ and 30 MPa. The obtained sample has a purity of 82.95 wt%, a relative density of 99.03%, and mean grain size of 12.46 μm in length and 5.12 μm in width. The main intermediate products during the reaction are Zr, $Zr_{0.75}S$, $ZrS_{0.67}$ and ZrB_2.

(2) The average thermal expansion coefficient of Zr_2SB at 200-1200 ℃ is 7.64×10^{-6} K^{-1}. The thermal diffusivity increases from 4.97 mm^2/s at room temperature to 7.29 mm^2/s at 1200 ℃. The thermal conductivity and heat capacity at room temperature are 12.0 $W \cdot m^{-1} \cdot K^{-1}$ and 0.39 $J \cdot g^{-1} \cdot K^{-1}$, respectively. The electrical conductivity at room temperature was determined to be 1.74×10^6 $\Omega^{-1} \cdot m^{-1}$.

(3) The flexural strength, fracture toughness and compressive strength were determined to be 269 ± 12.7 MPa, 3.94 ± 0.63 $MPa \cdot m^{1/2}$ and 2166.74 ± 291.34 MPa respectively. The Vickers hardness was determined to be 9.86 ± 0.63 GPa at 200 N. Excellent physical and mechanical properties give Zr_2SB the prospect as a functional-structural ceramic.

Acknowledgments

This work was supported by the Natural Sciences Foundation of China (52072311 and 52032011), Outstanding Young Scientific and Technical Talents in Sichuan Province (2019JDJQ0009), the Fundamental Research Funds for the Central Universities (2682020ZT61, 2682021GF013), the Opening Project of State Key Laboratory of Green Building Materials, and the Project of State Key Laboratory of Environment-Friendly Energy Materials (20kfhg17).

References

[1] Jeitschko W, Nowotny H, Benesovsky, F. Carbides of formula T_2MC. *J Less-Common Met* 1964, **7**: 133–138.

[2] Barsoum MW. The $M_{N+1}AX_N$ phases: A new class of solids. *Prog Solid State Chem* 2000, **28**: 201–281.

[3] Eklund P, Beckers M, Jansson U, Högberg H, *et al.* The $M_{n+1}AX_n$ phases: Materials science and thin-film processing. *Thin Solid Films* 2010, **518**: 1851–1878.

[4] Zhang Z, Duan X, Qiu B, *et al.* Preparation and anisotropic properties of textured structural ceramics: A review. *J Adv Ceram* 2019, **8**: 289–332.

[5] Hadi MA. Superconducting phases in a remarkable class of metallic ceramics. *J Phys Chem Solids* 2020, **138**: 109275.

[6] Sokol M, Natu V, Kota S, *et al.* On the Chemical Diversity of the MAX Phases *Trends Chem* 2019, **1**: 210–223.

[7] Chakraborty P, Chakrabarty A, Dutta A, *et al.* Soft MAX phases with boron substitution: A computational prediction. *Phys Rev Mater* 2018, **2**: 103605.

[8] Verger L, Kota S, Roussel H, *et al.* Anisotropic thermal expansions of select layered ternary transition metal borides: MoAlB, Cr_2AlB_2, Mn_2AlB_2, and Fe_2AlB_2. *J Appl Phys* 2018, **124**: 205108.

[9] Kota S, Chen Y, Wang J, *et al.* Synthesis and characterization of the atomic laminate Mn_2AlB_2. *J Eur Ceram Soc* 2018, **38**: 5333–5340.

[10] Zhang H, Dai F, Xiang H, *et al.* Crystal structure of Cr_4AlB_4: A new MAB phase compound discovered in Cr-Al-B system. *J Mater Sci Technol* 2019, **35**: 530–534.

[11] Guan CL. Rapid and low temperature synthesis of high purity Ti_2SC powder by microwave hybrid heating. *Adv Appl Ceram* 2016, **115**: 470-472.

[12] Zhou W, Liu L, Zhu J, *et al.* Facile synthesis of high-purity Ti_2SC powders by spark plasma sintering technique. *Ceram Int* 2017, **43**: 9363–9368.

[13] Zhu WB, Song JH, Mei BC. Kinetics and microstructure evolution of Ti_2SC during in situ synthesis process. *J Alloys Compd* 2013, **566**: 191-195.

[14] Hoseini SM, Heidarpour A, Ghasemi S. On the mechanism of mechanochemical synthesis of Ti_2SC from Ti/FeS_2/C mixture. *Adv Powder Technol* 2019, **30**: 1672–1677.

[15] Bouhemadou A, Khenata R. Structural, electronic and elastic properties of M_2SC (M=Ti, Zr, Hf) compounds. *Phys Lett A* 2008, **372**: 6448-6452.

[16] Fu H, Yang J, Zhao Z, *et al.* Static compressibility, thermal expansion and elastic anisotropy of Zr_2SC single crystals. *Solid State Commun* 2009, **149**: 2110–2114.

[17] Tomoshige R, Ishida K, Inokawa H. Effect of Added Molybdenum on Material Properties of Zr_2SC MAX Phase Produced by Self-Propagating High Temperature Synthesis. *Mater Res Proc* 2019, **13**: 79-84.

[18] Chen K, Chen Y, Zhang J, *et al.* Medium-entropy (Ti, Zr, Hf)$_2$SC MAX phase. *Ceram Int* 2021, **47**: 7582–7587.

[19] Feng W, Cui S, Hu H, *et al.* First-principles study on electronic structure and elastic properties of hexagonal Zr_2Sc. *Phys B: Condens Matter* 2010, **405**: 4294–4298.

[20] Music D, Sun Z, Schneider JM. Ab initio study of Nb_2SC and Nb_2S_2C: Differences in coupling between the S and Nb–C layers. *Solid State Commun* 2006, **137**: 306–309.

[21] Opeka M, Zaykoski J, Talmy I, *et al.* Synthesis and characterization of Zr_2SC ceramics. *Mat Sci Eng A* 2011, **528**: 1994–2001.

[22] Ali MA, Hossain MM, Uddin MM, *et al.* Physical properties of new MAX phase borides M_2SB (M = Zr, Hf and Nb) in comparison with conventional MAX phase carbides M_2SC (M = Zr, Hf and Nb): Comprehensive insights. *J Mater Sci Technol* 2021, **11**: 1000–1018.

[23] Rackl T, Eisenburger L, Niklaus R, *et al.* Syntheses and physical properties of the MAX phase boride Nb_2SB and the solid solutions $Nb_2SB_xC_{1-x}$ (x = 0–1). *Phys Rev Mater* 2019, **3**: 1–7.

[24] Rackl T, Johrendt D. The MAX phase borides Zr_2SB and Hf_2SB. *Solid State Sci* 2020, **106**:1–6.

[25] Qin Y, Zhou Y, Fan L, *et al.* Synthesis and characterization of ternary layered Nb_2SB ceramics fabricated by spark plasma sintering. *J Alloys Compd* 2021, **878**: 160344.

[26] Ghosh NC, Harimkar SP. Consolidation and synthesis of MAX phases by Spark Plasma Sintering

(SPS): a review. In *Advances in Science and Technology of $M_{n+1}AX_n$ Phases*. Low IM, 2012: 47–80.

[27] Anselmi-Tamburini U, Gennari S, Garay J, *et al.* Fundamental investigations on the spark plasma sintering/synthesis process. *Mat Sci Eng A* 2005, **394**: 139–148.

[28] Omori, M. Sintering, consolidation, reaction and crystal growth by the spark plasma system (SPS). *Mat Sci Eng A 2000,* **287**: 183–188.

[29] Lyu J, Kashkarov EB, Travitzky N, *et al.* Sintering of MAX-phase materials by spark plasma and other methods. *J Mater Sci* 2021, **56**: 1980–2015.

[30] Su X, Dong J, Chu L, *et al.* Synthesis, microstructure and properties of MoAlB ceramics prepared by in situ reactive spark plasma sintering. *Ceram Int* 2020, **46**: 15214–15221.

[31] Xu Q, Zhou Y, Zhang H, *et al.* Theoretical prediction, synthesis, and crystal structure determination of new MAX phase compound V_2SnC. *J Adv Ceram* 2020, **9**: 481–492.